nature communications

Article

https://doi.org/10.1038/s41467-026-75153-y

Preclinical characterization and phase 1 clinical testing of targeting mitochondrial peroxiredoxin 3 in cancer

Received: 1 June 2025

Accepted: 24 June 2026

Published online: 14 July 2026

Check for updates

Victoria Gibson[1,13], Joanna Dzialo[2,13], Terri Messier[1,13], Aleksandra Bzura[2,3], Charlotte Poile[2], Jan Rogel[2], Jens C. Hahne[2], Aida Habibovic[1], Stephanie Stead[1], Alexis Saaman[1], Kevin G. Blyth[4], Peter W. Szlosarek[5], Simon Lord[6], Fiona Thistlethwaite[7], Min Zhang[2,8], Apostolos Nakas[9], Peter Wells-Jordan[2], Kudzayi Kutywayo[2], Kelly J. Butnor[1], Nicholas. H. Heintz[1], George N. Naumov[10], Maurice Dungey[2,9], Julio Herrero Colomina[7], Burak Aktas[11], Sean Dulloo[2,9], James Spicer[11,14] ✉, Dean A. Fennell[2,9,14] ✉ & Brian Cunniff[1,10,12,14] ✉

Cancer cells counteract oxidative stress through upregulation of antioxidant networks. Peroxiredoxin 3 (PRX3), a mitochondrial antioxidant enzyme, regulates reactive oxygen species homeostasis and promotes tumor cell survival. The natural compound thiostrepton (TS) covalently inhibits PRX3, disrupting redox balance and selectively induces tumor cell death. Mesothelioma, an aggressive malignancy, has limited therapeutic options, particularly in relapsed or refractory settings. Here, we demonstrate genetic deletion of *PRX3* impairs mitochondrial bioenergetics and suppresses mesothelioma growth, while pharmacological inhibition of PRX3 with TS induces apoptosis in patient-derived mesothelioma explants. In a phase 1 trial treating patients with relapsed pleural mesothelioma and malignant pleural effusion (NCT05278975), weekly local intrapleural treatment with the TS formulated drug product RSO-021 at 90 mg is well tolerated leading to disease control in 67% of patients at 12 weeks and is associated with tumor reductions. Primary endpoints of safety, tolerability and dose finding were met, and secondary endpoints of pharmacokinetics, objective response rate, disease control rate, and progression free survival are explored. Genomic screening identified Solute Carrier Family 7 member 11 (SLC7A11) as a mediator of TS resistance, suggesting combined targeting may further enhance the pro-oxidant activity of RSO-021.

Oxidative stress is a hallmark of transformed cells which exist in a state of redox disequilibrium[1]. Tumorigenesis is associated with excessive production of reactive oxygen species (ROS), by-products of metabolism, surpassing the antioxidant buffering capacity of the cell[2,3]. ROS contribute to pro-tumorigenic signaling pathways, while excessive ROS accumulation induces macromolecular damage, lipid peroxidation, and cell death[4]. Mesothelioma, an aggressive cancer with limited treatment options[5], is associated with asbestos exposure, which drives ROS-mediated DNA damage and promotes oncogenic signaling[6,7].

At high levels, oxidative stress becomes tumor-suppressive, driving compensatory mechanisms in mesothelioma and other

A full list of affiliations appears at the end of the paper. ✉e-mail: james.spicer@kcl.ac.uk; df132@leicester.ac.uk; bcunniff@uvm.edu

https://doi.org/10.1038/s41467-026-75153-y

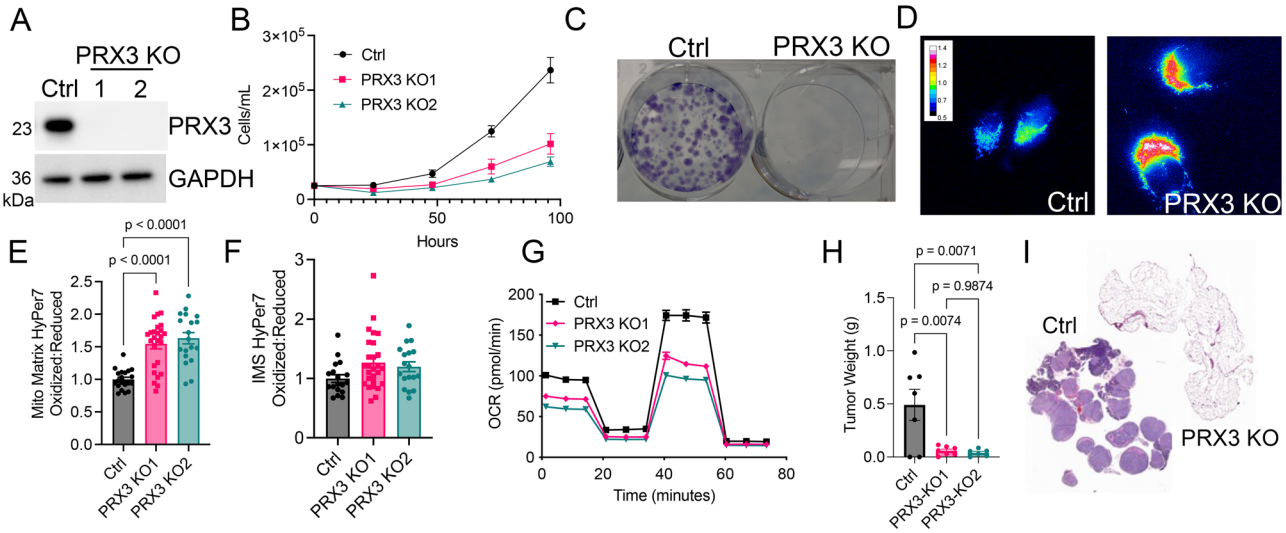

Fig. 1 | Peroxiredoxin 3 (PRX3) supports mesothelioma redox status, proliferation, and in vivo tumor growth. A PRX3 knockout human mesothelioma (H-MESO-1) cells (PRX3 KO Clone 1 (heterozygote) and PRX3 KO Clone 2 (homozygote)) were generated using CRISPR/CAS9. Western blot using PRX3 and GAPDH antibodies. **B** Cell proliferation of Ctrl and PRX3 KO cell lines ($n = 3$ independent experiments). **C** Representative images from colony formation assay of Ctrl and PRX3 KO Clone 2 cells. **D**. Representative mitochondrial localization sequence (MLS)-HyPer7 ratiometric images of Ctrl and PRX3 KO cells. Warmer colors indicate areas of increased MLS-HyPer7 oxidation. **E** Quantification of (MLS)-HyPer7 ratio ($n = 20$ cells per group). **F** Quantification of inner membrane space (IMS)-HyPer7 ratio ($n = 15$ cells per group). **G** Oxygen consumption rates using mitochondrial stress test assay ($n = 5$ independent experiments). **H** End-stage tumor weight at 41 days post tumor cell injection (n = 6 animals/group). **I** H&E staining of xenograft tumors from Ctrl and PRX3 KO xenografts. Data are presented as mean values +/− SEM. *P* values were determined by one-way ANOVA with Tukey's multiple comparison test.

cancers[8–10]. Mesothelioma tumor cells can be characterized as redox-driven tumors given the elevated levels of cellular ROS and increased expression of genes associated with escape from oxidative stress[7,9–13]. In mitochondria, the thioredoxin reductase 2 (TR2)–thioredoxin 2 (TRX2)–peroxiredoxin 3 (PRX3) axis serves as a dominant antioxidant system[14–16]. PRX3 scavenges hydrogen peroxide (H_2O_2) and is highly expressed in mesothelioma[17]. PRX3 is inhibited by the bacterial derived cyclic peptide thiostrepton (TS), which covalently inactivates PRX3 dimers through direct conjugation of active site cysteine residues[9,10,13,18]. The specificity of TS for PRX3 is partially driven by elevated pH and the likelihood of PRX3 to predominate as a dimer versus dodecamer in the mitochondrial matrix[18]. Our previous work identified mesothelioma tumor cells as being exquisitely sensitive to inhibition of the mitochondrial antioxidant TRX2/PRX3 network[9,11,13], supporting continued investigation into this approach for therapeutic intervention.

Here, we extend our previous findings demonstrating the tumor suppressive effects of PRX3 inhibition[9,10,13] by showing that CRISPR-based genetic and pharmacological targeting of PRX3 suppresses tumor growth in vitro and in vivo. We provide clinical evidence of safety and anti-tumor activity of TS formulated as RSO-021 in patients with relapsed pleural mesothelioma. Upregulation of Solute Carrier Family 7 member 11 (SLC7A11) confers resistance to PRX3 inhibition in mesothelioma cells and patient-derived surgical explants. These data highlight the importance of the redox equilibrium in tumor growth and the utility of redox disruption as a viable therapeutic strategy for treatment of mesothelioma and other cancers.

Results

Deletion of PRX3 is tumor suppressive

To investigate the functional role of *PRX3* expression in supporting mesothelioma growth we established CRISPR/Cas9 knockout of *PRX3* in the human biphasic mesothelioma cell line H-MESO-1, generating two clones, H-Meso$^{\Delta PRX3\text{-}1}$, a compound heterozygote deletion, and H-Meso$^{\Delta PRX3\text{-}2}$, a homozygote deletion (referred to as PRX3 KO clones) (Fig. 1A). Compared to mock CRISPR/Cas9 control cells, PRX3 KO clones exhibited a reduction in cell proliferation and ability to grow in colony formation assays (Fig. 1B–C). H-MESO-1 cells treated with TS (structure shown in Supplementary Fig. 1A) also show a dose-dependent decreased ability to form colonies (Supplementary Fig. 1B). Mitochondrial matrix H_2O_2 levels were evaluated with the genetically encoded mitochondrial localized oxidant sensor HyPer7[19] and found to be significantly increased in both PRX3 KO clones (Fig. 1D–E) while mitochondrial inner membrane targeted HyPer7 oxidation trended towards increased but did not reach statistical significance (Fig. 1F). In previous studies TS was shown to increase cellular and mitochondrial ROS by multiple experimental approaches[9,20]. Herein with the improved redox sensor HyPer7, we have validated those results (Supplementary Fig. 1C). Basal and maximum mitochondrial oxygen consumption rates (OCAR) as well as extracellular acidification rates (ECAR) were significantly reduced in both PRX3 KO clones (Fig. 1G and Supplementary Fig. 1D).

To assess in vivo tumor growth potential PRX3 KO and control cells were implanted in the peritoneal cavity of immunocompromised mice and end-stage tumor burden was determined after 41 days of growth. Both PRX3 KO clones failed to form measurable or histologically detectable xenografts in mice (Fig. 1H–I). In contrast, PRX3 expression in control cells was associated with extensive tumor burden (Fig. 1H–I). Together, *PRX3* deletion in H-MESO-1 cells inhibits tumor growth properties and elicits significant changes to the redox and metabolic status of mitochondria.

Thiostrepton (TS) induces apoptosis in patient-derived mesothelioma explants

Interrogation of the Cancer Dependency Map (DepMap)[21] showed that the small molecule PRX3 inhibitor TS efficiently reduced the viability of a panel of 578 human tumor cell lines (Supplementary Fig. 1E). TS induces cell death in the H-MESO-1 human mesothelioma cell line (Supplementary Fig. 1F) therefore, sensitivity to TS treatment was evaluated in 22 mesothelioma patient-derived explants (PDEs) collected during routine surgery as part of the MEDUSA cohort[22]. PDEs were treated ex vivo for 48 h with TS across multiple concentrations

(including 0 and 10 μM; Supplementary Fig. 1G). Cell death in tumor cells was quantified by multiplex immunofluorescence (mIF) using cleaved Poly (ADP-ribose) polymerase (cPARP) with pan-cytokeratin (PanCK) for tumor mask visualization, Ki67 for context, and DAPI for nuclei. Representative mIF paired images of media control and 10 μM TS-treated explants are shown in Fig. 2A. Treatment with TS caused heterogeneous cPARP induction across PDEs, indicating variable ex vivo apoptotic sensitivity to PRX3 inhibition (Fig. 2A–B). To capture this variability in a single, comparable metric – while accounting for the inherently heterogenous nature of mesothelioma tissue, variability of the PDE model, and unequal representation of analyzable tumor fragments across samples - we developed weighted response score (WRS) summarizing the integrated, multi-dose ability to induce cPARP after 48 h of TS treatment across all tested concentrations. Weighting by the number of explants and available treatment conditions was applied to reduce the potential risk of disproportionate influence from sparsely represented samples. Raw WRS values were then normalized by z-scoring relative to the cohort median and displayed in a waterfall plot (Fig. 2B), enabling ranking of PDEs by ex vivo apoptotic sensitivity. Responder (R) and Non-Responder (NR) groups were defined using a zero-centered threshold on the z-scored WRS ($R < 0$; $NR \geq 0$), giving two similarly sized groups for downstream analyses. Biologically, R reflected strong cPARP induction after TS treatment comparing to control, whereas NR represented relatively weaker or minimal induction. The underlying data used to derive this ranking and post hoc Dunn's comparisons of each TS concentration vs. control, which were not used to construct the WRS score, are provided in Supplemental Data 1 in the supplementary information. Kaplan–Meier survival analyses showed no significant difference in overall survival (OS: HR = 1.35, 95% CI: 0.36–5.04, $p = 0.66$) or progression free survival (PFS: HR = 0.65, 95% CI: 0.26–1.66, $p = 0.37$) between patients donating R and NR explants (Fig. 2D). The absence of significant differences in baseline OS/PFS between tissue donors from R and NR groups suggests no baseline survival differences between WRS-defined R and NR groups. A genomic heatmap created for the most frequently affected genes in mesothelioma as well as for genes putatively relevant to response to PRX3 inhibition, highlighted two candidates for further investigation (Fig. 2C). Notably, copy number alterations involving 3p21.31 comprising BRCA1 associated protein 1 (*BAP1), and* SET domain containing 2 (SETD2), a region commonly altered in mesothelioma, were associated with increased cPARP induction following PRX3 inhibition (Fig. 2C, E–F). Losses, deletions, and mutations in the *BAP1* and *SETD2* genes were significantly more frequent in PDEs from R group (Fig. 2E–F, Fisher tests; $p = 0.0124$ for *BAP1*, $p = 0.03$ for *SETD2*).

Clinically formulated TS (RSO-021) is tolerable with evidence of clinical response

TS was formulated as RSO-021 (3 mg/ml TS, 5% VitE-TPGS, 2% DMSO in saline) for clinical administration and evaluated in a first-in-class, phase 1 clinical trial using a 3 + 3 study design (MITOPE, NCT05278975). Eligible patients had a malignant pleural effusion (MPE) with an indwelling pleural catheter (IPC) to enable local delivery of RSO-021 into the pleural space and tumor disease measurable by the modified Response Evaluation Criteria in Solid Tumors version 1.1 (mRECIST1.1). All patients had previously progressed following prior systemic therapy. Additional eligibility criteria are detailed in the study protocol (Supplementary Information) and patient baseline characteristics are summarized in Supplementary Table 1.

RSO-021 was administered locally to the pleural space via an IPC, once weekly (21-day cycle, no breaks between treatment cycles) as a monotherapy until radiological progression. A total of 15 patients (12 pleural mesothelioma, one colorectal cancer, two non-small cell lung cancer) were treated as part of this phase 1 clinical trial. All dosed pleural mesothelioma patients had diagnosed epithelioid disease associated with pleural effusion and had failed standard of care treatment. Dose-limiting toxicity (DLT) was defined as one or more of the following events occurring during the first cycle (21 days) of administration of RSO-021: any Grade (Gr). ≥3 non-hematological treatment emergent adverse events (TEAEs) or Gr. 4 neutropenia, febrile neutropenia, Gr. 4 anemia, Gr. 3/4 thrombocytopenia according to CTCAE V5.0. No DLTs were observed among the seven patients treated at the 90 mg dose level. Two DLTs were observed in two of the six treated patients at the 120 mg level (Gr. 3 acute inflammatory response and Gr. 3 shortness of breath) and one DLT (Gr.3 dyspnea) in the two patients treated at the 180 mg dose level (Supplementary Table 2). The most common TEAEs included fatigue (all dose levels: 33.3%, 90 mg cohort: 28.6%), pyrexia (all dose levels: 20%, 90 mg: 14.3%), pain (all does levels: 13.3%, 90 mg: 0%), anemia (all dose levels: 13.3%, 90 mg: 14.3%), cough (all dose levels: 13.3%, 90 mg: 14.3%), and hypotension (all dose levels: 13.3%, 90 mg: 0%) (Supplementary Table 2 & 3). Almost all observed TEAEs were grade 1 or 2.

The measured systemic plasma concentration of TS during the first 24 h after local intrapleural administration was 1000-fold lower than the administered doses and was slightly above the detection limit of the assay (Fig. 3A). No significant systemic drug was observed in the plasma past the first 24 h after administration. In contrast, pleural concentrations of TS increased over the first 3 weekly doses to a steady state of 10,000 ng/ml when measured in the removed pleural fluid prior to the weekly RSO-021 administration at 90 mg (Fig. 3B).

A partial response was observed in one of 10 evaluable patients (10%) in the 90 mg treatment cohort (Fig. 3C–E). By 12 weeks the disease control rate was observed in 6 out of 9 evaluable patients (67%), comprising one with partial response and five with stable disease by mRECIST1.1 (Fig. 3C–D). The partial response observed at the 90 mg dose level exhibited durability lasting until week 30 (Fig. 3E), measured at the time of the first response assessment at 6 weeks, with further evidence of tumor reduction by week 17 (Fig. 3E, nadir of 60.7%).

The volume of pleural effusion was reduced over the course of treatment for most patients (Fig. 3F–G). At the time of tumor progression, pleural drainage volumes were significantly reduced from a median of 700 ml/week (pre-treatment) to a median of 175 ml/week (at the time of treatment discontinuation) (Fig. 3F). Median PFS was 18 weeks ($n = 9$ patients, assessable efficacy population), and OS was not reached by 80 weeks (n = 12 patients) in this relapsed mesothelioma cohort (Fig. 3H–I). PRX3 covalent crosslinking by RSO-021 was observed in two patient-derived pleural effusions 24 h post 2nd dose (C1D9) of RSO-021 (Fig. 3J), validating TS activity in human tissue.

SLC7A11 mediates resistance to PRX3 inhibition

To identify agents that modulate TS sensitivity, a drug screen of potentially synergistic interactions was examined in H-MESO-1 cells using a panel of experimental compounds known to influence cellular metabolic and redox status (Supplementary Fig. 2A–B). We quantitatively determined drug-drug interactions (antagonistic, additive, or synergistic) using the Zero Interaction Potency (ZIP) model for unbiased identification of synergistic relationships[23]. Of the 8 compounds screened in combination with the PRX3 inhibitor TS for 48 h, erastin showed the greatest level of synergy as defined by a ZIP synergy score (ZSS) of 14.58 and was confirmed in a second mesothelioma tumor cell line (Fig. 4A–B and Supplementary Fig. 2B–C).

Erastin is an irreversible inhibitor of System Xc/SLC7A11, a plasma membrane antiporter that imports reduced cysteine (cystine) in exchange with export of glutamate[24]. Erastin when used in combination with TS potentiated PRX3 crosslinking, cellular ROS levels (Fig. 4C–E) and elicited a significant drop in cellular glutathione (GSH) levels compared with TS alone (Supplementary Fig. 2D).

Depletion of cystine from the cell culture media also potentiated TS cytotoxic activity and PRX3 crosslinking (Fig. 4F–G). Depletion of cystine and erastin are strongly linked with induction of ferroptosis, a mode of cell death driven by lipid oxidation[25]. Co-treatment with the

https://doi.org/10.1038/s41467-026-75153-y

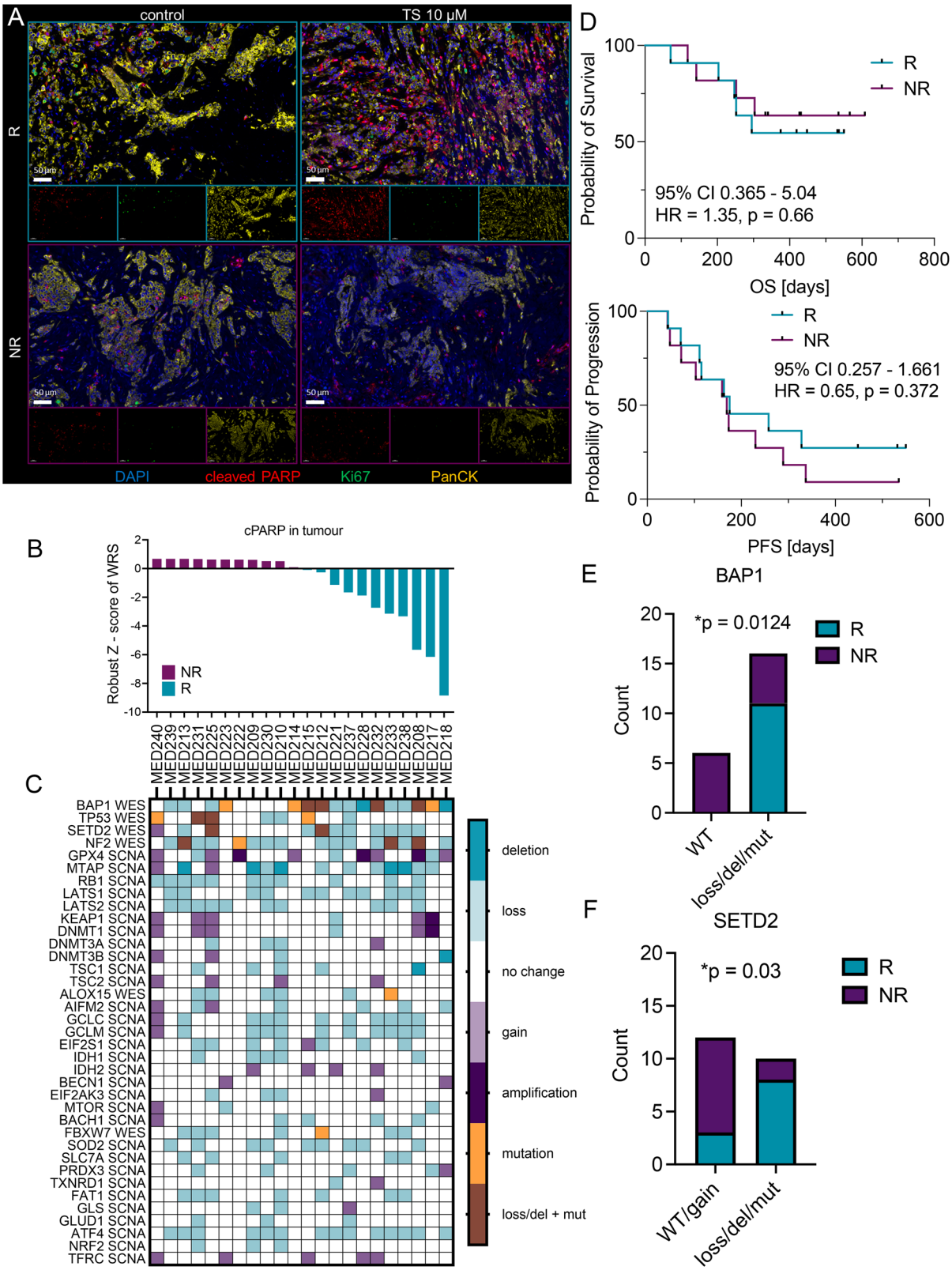

ferroptosis inhibitors Ferrostatin-1 (Fer-1) or Liproxstatin-1 (Lip-1) blocked erastin cytotoxicity but were unable to block TS activity (Supplementary Fig. 3A–D). Fer-1 or Lip-1 did not block synergy effects of TS with erastin or increase PRX3 crosslinking by erastin (Supplementary Fig. 3E–F).

To further confirm the impact of cystine import and cellular responses to erastin, SLC7A11 was silenced using RNA interference (siRNA) and responses to TS evaluated (Fig. 4H and Supplementary Fig. 4A–B). Cells with SLC7A11 knockdown via siRNA were significantly more sensitive to TS (effective cytotoxic concentration (EC_{50}) of 0.27 µM, Fig. 4I) compared with scrambled control (EC_{50} of ~1 µM, Fig. 4I). TS-induced PRX3 crosslinking was increased in cells with silenced SLC7A11 (Supplementary Fig. 4C–D).

https://doi.org/10.1038/s41467-026-75153-y

Fig. 2 | Antitumor activity of thiostrepton (TS) in a co-clinical PDE model of mesothelioma. A Representative multiplex fluorescent immunohistochemistry (mIF) images of explant samples from WRS-defined Responder (R,top panel) and Non-Responder (NR,bottom panel) groups. Merged images show the co-localization of markers: cleaved poly (ADP-ribose) polymerase-1 (cPARP) (red), Ki67 (green), pan-cytokeratin (PanCK) (yellow), nuclear stain-DAPI (blue). Individual channels for cPARP, Ki67 and PanCK are displayed below the merged images. Images correspond to untreated (media control) and 10 μM TS-treated conditions. **B** cPARP levels, quantified from mIF staining of explants across multiple TS concentrations (5, 10, 100 μM), along with statistical analysis results (Kruskal–Wallis rank-sum test), were used to calculate the Weighted Response Score (WRS). The WRS, normalized using a robust Z-score method, served as the basis for stratifying samples into R and NR groups. Explants with a normalized WRS value below 0 were assigned to R (teal), while those with values above 0 were designated as NR (purple). **C** Heatmap illustrating genomic alterations in key mesothelioma-specific and TS treatment-relevant genes across R and NR groups. Genomic alterations include deletions (dark teal), losses (light teal), gains (light purple), amplifications (dark purple), mutations (orange), and double-hit events involving both mutation and loss (brown). **D** Kaplan–Meier survival curves comparing progression-free survival (PFS, top panel) and overall survival (OS, bottom panel) in patients from MEDUSA cohort, whose tumors were categorized as R (teal) or NR (purple), based on ex vivo explants analysis. PFS and OS represent clinical outcomes for these patients, in the absence of TS treatment (log-rank [Mantel–Cox] test, censored as of August 2024). **E–F** Genomic alterations in BAP1 and SETD2 were analyzed to assess enrichment in R (teal) and NR (purple) groups. Statistical comparisons were performed using a two-sided Fisher's exact test. *N = 22 independent patient samples for 2D-F.*

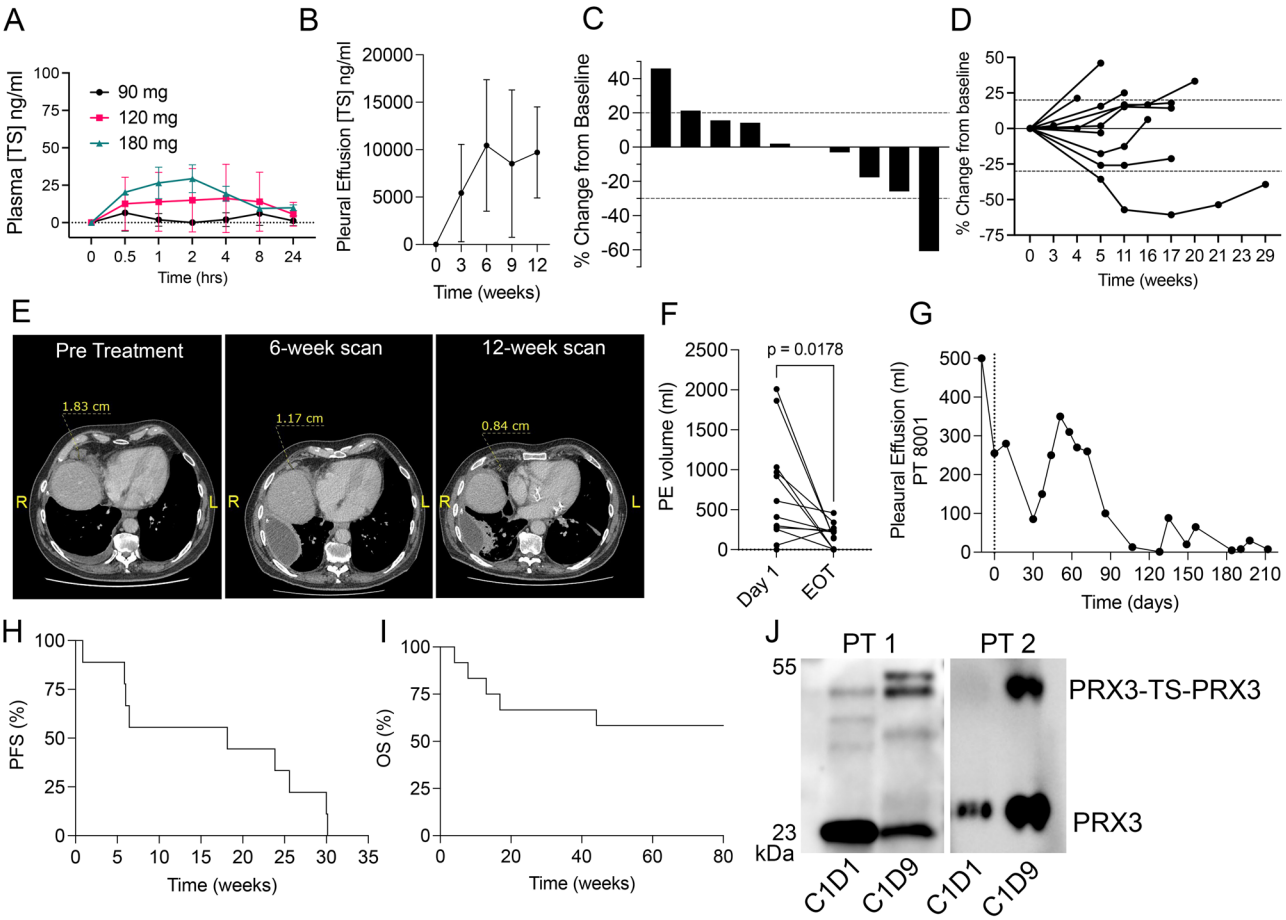

Fig. 3 | A clinical formulation of TS (RSO-021) is safe, tolerable and exhibits signals of efficacy in humans. A Plasma levels of TS at indicated timepoints from patients treated with 90 mg, 120 mg or 180 mg dose RSO-021 ($n = 7$ for 90 mg, $n = 3$ for 120 mg, and $n = 2$ for 180 mg groups, a total of 15 patients had plasma TS assessed, but only 7 patients had detectable TS). Data are presented as mean values +/- SEM**. B** Levels of TS in pleural effusions at indicated times (weeks) from patients treated with a 90 mg dose of RSO-021 ($n = 5$ at 0 weeks, $n = 3$ at 3 and 12 weeks and $n = 4$ at 6 and 9 weeks). Note significant distribution in data due to variable collection of effusion volume between patients. Data are presented as mean values +/− SEM**. C** Waterfall plot showing best mRECIST v1.1 response for patients treated with RSO-021 ($n = 10$ total evaluable patients, 6 patients at 90 mg, 3 patients at 120 mg and 1 patient at 180 mg). **D** Spider plot showing percentage change in mRECIST v1.1 from baseline for patients (same as patients shown in **C**) treated with RSO-021 ($n = 10$ patients). Note: X-axes are not linear. **E** CT-scan from patient with partial response in disease at the right cardiophrenic angle, at baseline prior to RSO-021, and after 6 and 12 weeks on treatment. Note differences in anatomical landmarks may affect the appearance of structures near the lung bases across scans. **F** Volume of pleural effusion drained from individual patients at baseline (pre - and 24 h - post first dose of RSO-021) and at end of treatment (EOT) ($n = 11$ samples, P value determined by Students *t*-test, change in mean volume). **G** Pleural effusion drainage from the patient presented in (**E**). Treatment with RSO-021 initiated at the vertical dotted line. **H** Progression free survival (PFS) of mesothelioma patients only, all dose levels ($n = 9$ patients). **I** Overall survival (OS) of mesothelioma patients only ($n = 12$ patients, 7 patients remain alive at time of data cutoff (80 weeks). **J** TS induced PRX3 crosslinking in patient-derived pleural effusions as determined by protein western blotting with PRX3 antibody in 2 individual patients 24 h after receiving their 2nd dose of RSO-021 (day 9).

https://doi.org/10.1038/s41467-026-75153-y

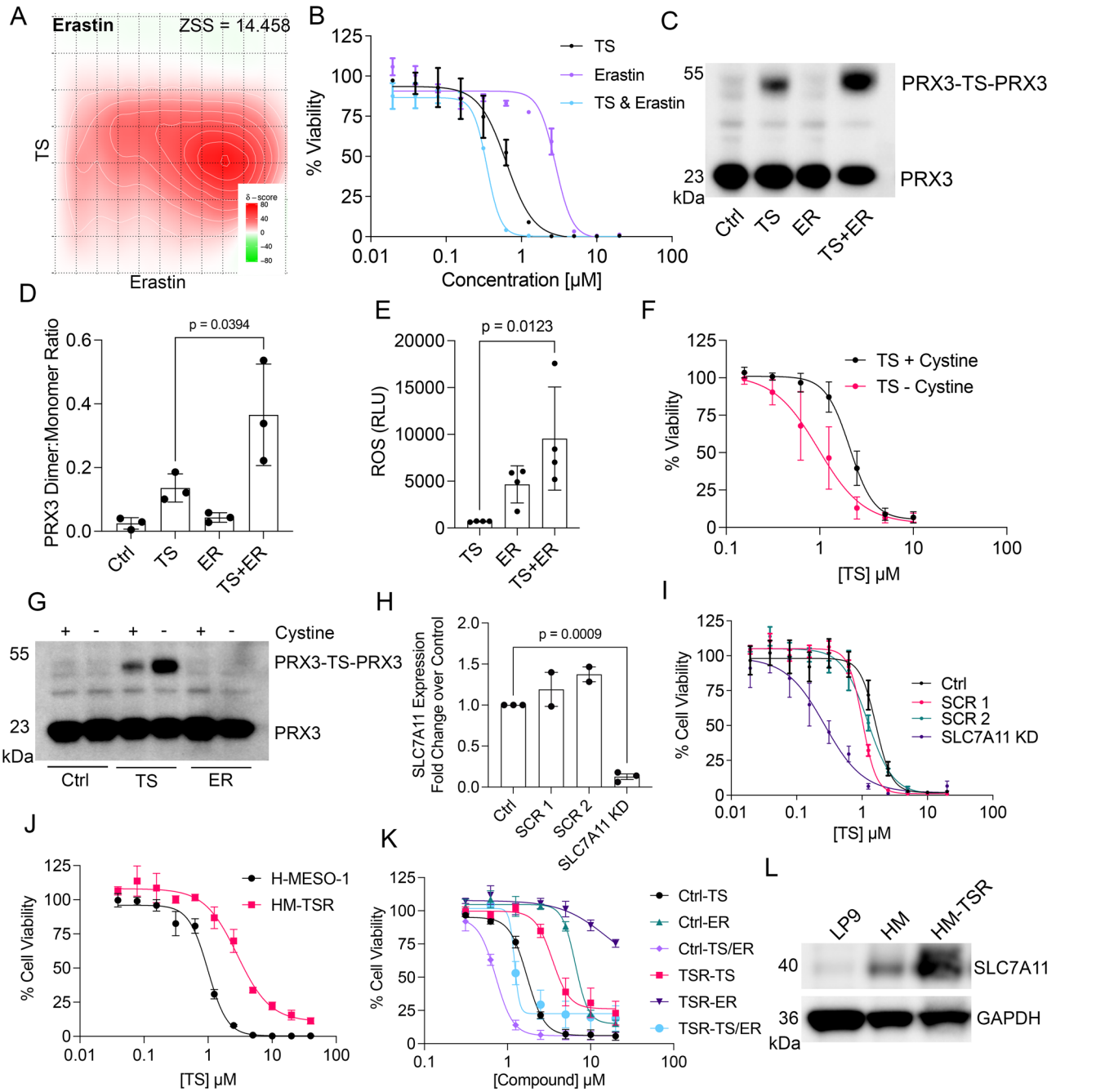

Fig. 4 | SLC7A11 - A putative biomarker of thiostrepton resistance. A Synergy distribution plot and Zip Synergy Score (ZSS) of erastin (ER) tested in combination with TS. **B** Sensitivity of H-MESO-1 cells to TS, ER or TS + ER ($n = 3$ independent experiments). **C** Western blot from H-MESO-1 cells treated with TS (1 μM), ER (2.5 μM) or TS + ER for 24 h. Samples were run under reducing conditions by SDS-PAGE. **D** Quantification of PRX3 dimer (TS-covalent crosslink) to PRX3 monomer (unmodified PRX3) from protein western blots as in shown in **C** ($n = 3$ independent experiments). **E** Reactive oxygen species (ROS) levels in cells treated with TS, ER or TS + ER for 24 h ($n = 4$ independent experiments). **F** Cell viability curves of H-MESO-1 cells treated with TS in media +/- cystine supplementation ($n = 4$ independent experiments, 3 technical replicates). **G** Protein western blot of H-MESO-1 cells cultured in media +/− cystine and treated with TS or ER. Note PRX3 covalent crosslinking by TS is increased in cells cultured in cystine free media. **H** SLC7A11 mRNA expression in H-MESO-1 control (Ctrl), siRNA scramble controls (SCR1 and SCR2) and siSLC7A11 H-MESO-1 cells after a 24-h incubation ($n = 3$ independent experiments). **I** Cell viability assay of H-MESO-1 cell line with indicated permutations treated with TS ($n = 3$ independent experiments). **J** Cell viability assay of H-MESO-1 and HM-TSR (TS-resistant) cells treated with TS for 48 h ($n = 3$ independent experiments). **K** Cell viability assay of H-MESO-1 and HM-TSR cells treated with TS, ER or TS + ER for 48 h ($n = 4$ independent experiments, 3 technical replicates). **L** Western blot of SLC7A11 levels in LP9 (immortalized human mesothelioma cells), H-MESO-1 and HM-TSR cells. Data are presented as mean values +/− SEM. *P* values were determined by one-way ANOVA with Tukey's multiple comparison test.

Next, a TS resistant H-MESO-1 cell line was generated (HM-TSR) with an EC_{50} of ~ 3.1 μM versus EC_{50} ~ 0.8 μM in the parental cell line (Fig. 4J and Supplementary Fig. 4). HM-TSR cells grew significantly slower than parental H-MESO-1 cells (Supplementary Fig. 4E) and were resistant to erastin (Fig. 4K). H-MESO-1 cells had higher SLC7A11 protein levels compared to normal immortalized LP9 mesothelial cells and HM-TSR cells had significantly higher SLC7A11 protein levels compared to parental H-MESO-1 cells (Fig. 4L). HM-TSR cells were re-sensitized to TS when treated in combination with erastin (Fig. 4K).

SLC7A11 expression is higher in WRS-defined NR mesothelioma PDEs

SLC7A11 expression was significantly higher at baseline in WRS-defined NR PDEs, as determined by DESeq2 analysis (padj=0.0021) (Fig. 5A) and confirmed by the Mann–Whitney test (Fig. 5B). Paired RNA analysis demonstrated significant induction of SLC7A11 mRNA in TS-treated samples compared with media control (Fig. 5C, Wilcoxon $p < 0.0001$). Representative mIF images illustrate higher SLC7A11 immunofluorescent signal in TS-treated explants relative to media control from the same donor tissue (Fig. 5D–E).

To explore the prognostic relevance of SLC7A11 and PRX3 in an external dataset, Kaplan-Meier survival analysis using median splits was performed in the TCGA MESO RNAseq data (Supplementary Fig. 5A–B). Higher SLC7A11 expression was significantly associated with shorter OS, an effect that was recapitulated in our explant cohort for OS as well as for PFS (Supplementary Fig. 5A–C). No significant association was observed for PRX3 expression in either dataset (Supplementary Fig. 5B–D).

Interestingly, SLC7A11 showed prognostic potential in both cohorts (TCGA–MESO and TS-treatment PDE cohort from MEDUSA) when stratified by median expression, but this association was not reproduced when cases were grouped according to WRS R/NR split. This suggests that baseline SLC7A11 expression captures only part of the variability reflected by the WRS-defined grouping. To further explore the relationship between gene expression, clinical outcome, and PDE-derived functional metrics, Spearman correlation analyses were performed for SLC7A11 (Supplementary Fig. 5E) and PRX3 expression (Supplementary Fig. 5F) vs. post-surgery OS, PFS, and z-scored WRS values in the MEDUSA cohort. No significant associations were observed for either marker (Supplemental Fig. 5E–F).

Pathway analysis using Hallmark gene sets performed on baseline PDE donor tissue stratified according to the WRS-defined R and NR groups revealed enrichment of innate immunity-related pathways in R samples (e.g., interferon gamma response, interferon alpha response). In contrast, NR samples showed relative enrichment of stress response pathways (e.g., hypoxia, reactive oxygen species) and proliferation – associated programs (e.g., MYC targets V1/V2, G2M checkpoint, E2F targets) (Fig. 5F). These findings provide additional molecular context for baseline differences between WRS-defined groups.

Discussion

Here, we show that either *PRX3* knockout or pharmacological inhibition of PRX3 is tumor suppressive in vitro and in vivo in mesothelioma models. Additionally, targeting PRX3 is feasible in the clinic, exhibiting tolerability and evidence of radiological response. Collectively, our findings suggest that oxidative stress modulation may be a viable therapeutic avenue in mesothelioma, a disease characterized by intrinsic redox disequilibrium[7,10,13,26].

PRX3 knockout causes a profound impairment in tumor growth, consistent with previous reports implicating PRX3 as a key mitochondrial antioxidant that sustains tumor cell survival under oxidative stress conditions[10,27,28]. Elevated mitochondrial H_2O_2 levels in PRX3 KO cells underscore its role in buffering redox imbalances, while the observed decrease in oxygen consumption and extracellular acidification rates suggests a broader disruption of mitochondrial function. Previously, using shRNA against PRX3 we reported an increase in OCAR and ECAR parameters alongside elongation of mitochondrial networks[10]. These conflicting observations may be attributed to compensatory mechanisms in place when partial PRX3 expression remains but warrants further investigation. Regardless, both findings are supported by reports showing that PRX3 expression correlates with metabolic adaptation and resistance to oxidative stress[9,13]. In addition, our PRX3 KO results fit with previous biochemical and modeling studies that predict the non-redundancy and pivotal role of PRX3 in buffering matrix H_2O_2 levels[15]. Data from the DepMAP pooled CRISPR-CAS9 screens processed using the "Chronos" algorithm (DepMap, Broad (2025). DepMap Public 25Q3. Dataset[29]) shows the dependency for PRX3 expression across numerous tumor types (Supplementary Fig. 6). Importantly, *PRX3* knockout is not embryonic lethal and has only minor phenotypes such as adipocyte hypertrophy[30,31]. The widespread expression of PRX3 in tissues and its elevated levels found in certain cancers[32,33], highlight a potential vulnerability to PRX3 inhibition as a therapeutic strategy.

In vivo, the complete absence of tumor formation in *PRX3* KO xenografts underscores the essential role of PRX3 in mesothelioma progression. PRX3 is a pro-survival factor protecting cells from H_2O_2 induced apoptosis[27], and based on our results, a targetable vulnerability. Not only in cell lines, but also patient-derived tumor explants, and in the clinic.

We evaluated a clinical formulation of TS (RSO-021) in a phase 1 clinical trial (MITOPE, NCT05278975). The pleural space has been highlighted as a potential route for therapy for mesothelioma[34] and was the chosen route of administration of RSO-021. Intrapleural administration provides a unique opportunity for repeated sampling of tissue for translational research and the ability to administer increased drug levels locally without significant systemic exposure. RSO-021 was administered into the pleural space of patients with MPE; mainly mesothelioma or other solid tumors metastatic to the pleura including colorectal and non-small cell lung cancer. The trial demonstrated that intrapleural administration of RSO-021 was well tolerated, with DLTs emerging only at higher dose levels. Notably, PRX3 dimerization—an established marker of target engagement—was detected in pleural effusions, confirming on-target drug activity. Furthermore, the reduction in pleural effusion volumes in most patients is in line with previous evidence of effusion management from IPC placement[35] and therefore not suggestive of drug-mediated effects. The observation of durable responses, safe administration, a manageable toxicity profile, and target engagement supported transition of RSO-021 to phase 2 testing (NCT05278975).

SLC7A11 was identified as a critical mediator of resistance to PRX3 inhibition, highlighting the therapeutic potential of combined targeting strategies to enhance treatment efficacy. Erastin, a SLC7A11 inhibitor exhibited potent synergy with TS suggesting that cystine import could play a central role in buffering oxidative stress induced by PRX3 inhibition. The ability of erastin to potentiate PRX3 cross-linking and ROS accumulation, while simultaneously depleting GSH, underscores the interplay between mitochondrial and cytosolic redox systems in dictating mesothelioma cell fate. Increased SLC7A11 expression was observed in mesothelioma cell lines with generated TS resistance (HM-TSR) and mesothelioma PDEs with increased SLC7A11 expression were less sensitive to TS. Moderate SLC7A11 overexpression has been reported in some cancers to mediate ferroptosis resistance[36–39] while high SLC7A11 expression sensitizes tumor cells to hydrogen peroxide[40]. Our finding, that TS induces upregulation of SLC7A11 in PDEs and patient samples, suggests that SLC7A11 expression may act as inducible adaptation to PRX3 inhibition, most likely through elevated mitochondrial oxidative stress.

BAP1 and SETD2 loss, deletion, or mutation were associated with apoptosis induction in TS-treated mesothelioma PDEs. BAP1 is frequently inactivated in mesothelioma[41–45]; its normal tumor suppressor function is coupled to and plays a role in induction of ferroptosis, via repression of the oxidant cystine transporter SLC7A11 via histone H2A ubiquitination[46]. We did not observe protection from TS by ferroptosis inhibitors, therefore, we hypothesize TS is not inducing ferroptosis but TS sensitivity is associated with signaling related to ferroptosis. Regardless, BAP1 mutant mesotheliomas may be more sensitive to RSO-021 and warrants clinical evaluation. BAP1 deficiency enriches immune-associated pathways in mesothelioma including the interferon alpha/gamma response[47]. This increased

https://doi.org/10.1038/s41467-026-75153-y

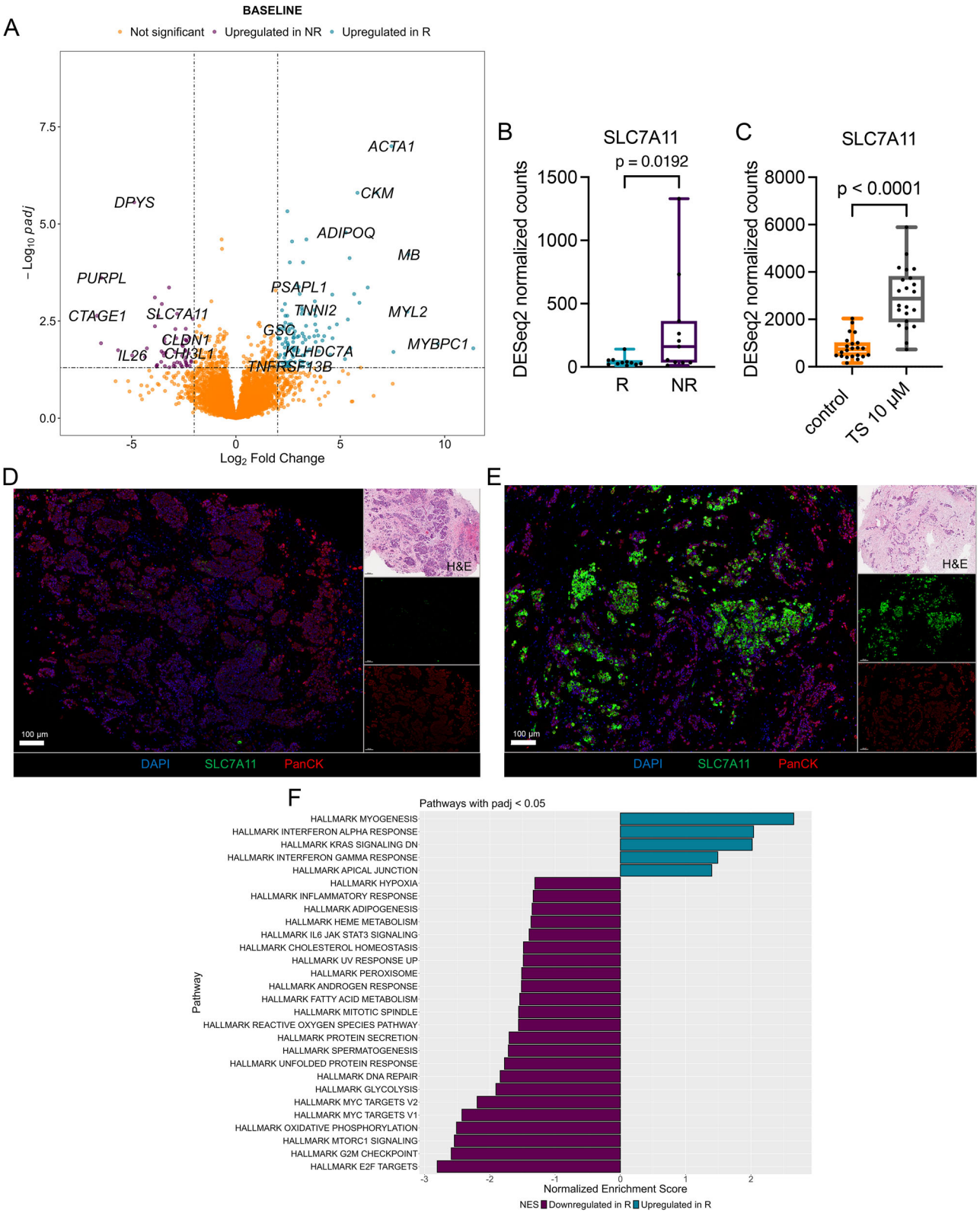

immunogenic microenvironment may play a role in sensitizing BAP1 deficient tumors to increased oxidative stress induced by TS. SETD2 is often found co-mutated with BAP1 due to chromosomal location and functions as a tumor suppressor via regulation of multitude cellular pathways[48]. SETD2 activates Ataxia-telangiectasia mutated (ATM) DNA damage response following oxidative insults to support repair of 8-hydroxyguanine lesions and is enriched at promoter regions in response to oxidative DNA damage[49,50]. Cells lacking SETD2 fail to trigger H_2O_2-induced ATM activation and accumulate 8-hydroxyguanine lesions[49]. This implies that SETD2 mutant tumors could be exploited therapeutically with the pro-oxidant strategy of PRX3 inhibition.

Our findings raise several key questions for future investigation. First, given that SLC7A11 upregulation emerges as a resistance mechanism, combining PRX3 inhibitors with ferroptosis-inducing agents such as erastin or glutathione peroxidase 4 (GPX4) inhibitors

Fig. 5 | SLC7A11 expression is associated with reduced TS-induced apoptosis in mesothelioma PDEs. A Volcano plot summarizing differential gene expression analysis performed on baseline (untreated, uncultured) tissue from donors in the MEDUSA cohort. Tumor groups (WRS-based R and NR) were defined by the outcome of ex vivo explant treatment with 10 μM TS. The *x*-axis represents log2 fold change in gene expression (R versus NR), and the y-axis shows -log10 adjusted p-values. Genes significantly upregulated in NR group (shown on the left, negative fold change) are highlighted in purple, while those upregulated in R group (shown on the right, positive fold change), are in teal. Differential expression analysis was performed using DESeq2 with two-sided Wald tests. *P* values were adjusted for multiple testing using the Benjamini–Hochberg method. $N = 22$ patient samples. **B** Expression of SLC7A11 at baseline in R and NR groups, measured as DESeq2 normalized counts. Statistical comparison was performed using the Mann–Whitney U test ($n = 22$ patient samples). **C** SLC7A11 expression measured as DESeq2 - normalized counts in explants exposed ex vivo to TS (10 μM) vs. donor-matched media control explants. (Wilcoxon signed- rank test) ($n = 22$ patient samples). In the box plots, the central line represents the median, boxes indicate the interquartile range (25th–75th percentiles), and whiskers extend to the minimum and maximum values. **D** Representative images of control and (**E**) TS (10 μM) treated explants from the same donor for SLC7A11 (green), PanCK (clone MNF116, red) and nuclei with DAPI (blue). Side panels show single marker staining and corresponding H&E images from matched explants on adjacent sections, highlighting tumor morphology and marker distribution. Staining was performed once per sample on tumor sections from a subset of independent patients. Representative images are shown. **F** Gene set enrichment analysis (GSEA) of pathway level differences between R and NR tumors in the MEDUSA cohort in baseline (untreated, uncultured) tissue gene expression profiles. The bar plot displays pathways with adjusted $p < 0.05$, with Normalized Enrichment Scores (NES) shown on the x-axis. Pathways enriched in R are highlighted in teal, while pathways downregulated in R (upregulated in NR) are in purple.

warrants further exploration. Clinically available SLC7A11 inhibitors including sorafenib[24] and sulfasalazine[51], may be a clinically actionable strategy for potentiating PRX3 inhibition. Sorafenib has shown moderate activity in mesothelioma[52] but has also been shown to minimally induce ferroptosis in other studies[53]. Secondly, PRX3 inhibition may have useful activity beyond mesothelioma or cancers with MPE but would require systemically bioavailable PRX3 inhibition, work currently underway[54]. In this setting, our finding that PRX3 dimerization occurs in patients' pleural effusions, suggests its potential as a pharmacodynamic biomarker to support optimal biological dosing of systemic PRX3 inhibition in future trials.

In summary, PRX3 inhibition is a tractable therapeutic target in mesothelioma. SLC7A11 confers resistance and is dynamically regulated following PRX3 inhibition, suggesting adaptive redox responses. Future studies will be required to extend PRX3 inhibition beyond the pleural space with systemic formulations, and to explore rational combination strategies aimed at enhancing therapeutic oxidative stress induced tumor suppression.

Methods

All research conducted within complies with all state and federal regulations

Cell studies were approved by the University of Vermont Institutional Biosafety Committee. All protocols used in animal experiments were approved by the University of Vermont Institutional Animal Care and Use Committee. For each study patient, written informed consent was obtained prior to any protocol-related activities. All research conducted with patient samples was approved by the University of Vermont Institutional Review Board (IRB) and the University of Leicester Research Ethics Committee.

Cell lines

Experiments were conducted using a series of human mesothelioma cell lines (H-MESO-1, HM-TSR (TS resistant H-MESO-1), PRX3 KO1 (compound heterozygous), PRX3 KO2 (homozygous), PRX3 Ctrl (mock transfected control) and a normal mesothelial cell line, LP9 (TERT-immortalized normal mesothelial cell line). PRX3 KO cell lines were generated through CRISPR/Cas9 (Synthego, Redwood City, CA, USA) using guide RNA sequence UUCCACAUGCAGCAGGCCUG, targeting exon 2 at the cut location Chr10:119,177,098. Cells were regularly tested for *Mycoplasma* contamination using PCR. Cell line authentication was completed by the Vermont Integrative Genomics Resource Core using the Promega GenePrint 10 System according to the manufacturer's instructions (Cat# B9510, Promega, Madison, WI, USA). Results were compared to known short tandem repeat fingerprints in Cellosaurus https://web.expasy.org/cellosaurus/ or compared against the H-MESO-1 parental cell line.

Chemicals and compounds

Metabolic inhibitors: 2-Deoxyglucose (2-DG) (Cat# D8375, Sigma-Aldrich, St. Loius, MO, USA), Dichloroacetate (DCA) (Cat# AC33828, Acros Organics, Fair Lawn NJ, USA) and CPI-613 (Devimistat) (Cat# 2125, Axon Medchem, Reston, VA, USA).

ROS modulators: 2,3-dimethoxy-1,4-naphthoquinone (DMNQ) (Cat# AG-CR1-3598-M005, AdipoGen Life Sciences, San Diego, CA, USA), Menadione (MD) (Cat# M5625, Sigma-Aldrich, St. Loius, MO, USA) and Elesclomal (Cat# S1052, Selleckchem, Houston, TX, USA). GSH modulators: Erastin (Cat# E7781, Sigma-Aldrich, St. Loius, MO, USA), and TLK-199 (Cat# 16248, Cayman Chemicals, Ann Arbor, MI, USA). GPX inhibitor: RSL3 (Cat# 19288, Cayman Chemical, Ann Arbor, MI, USA). Antioxidants: Ferrostatin-1 (Fer-1) (Cat# A4371, APExBIO, Boston, MA, USA), Liprostatin (Lip-1) (Cat# 6113, Tocris, Minneapolis, MN, USA), Thiostrepton (TS) (Cat# 598226, Calbiochem/Millipore, Boston, MA, USA), Gentian violet (Cat# 1290002, Sigma-Aldrich, St. Louis, MO, USA).

Cell growth conditions

Cell lines were adapted and grown in DMEM:F12 (Cat# 10-092, Mediatech, Manassas, VA, USA) supplemented with 10% Fetal Bovine Serum (FBS) (Cat# 26140-079, Gibco, Grand Island, NY, USA), Hydrocortisone (Cat# H0135, Sigma, St. Louis, MO, USA), and Insulin-Transferrin-Selenium (Cat# 41400-045, Gibco, Grand Island, NY, USA). Cystine-depleted experiments were conducted using DMEM (Cat# 21012-024, Gibco, Grand Island, NY, USA) with added L-glutamine (Cat# 25030-081, Gibco, Grand Island, NY, USA), Sodium Pyruvate (Cat# 11360-070, Gibco, Grand Island, NY, USA), L-Methionine (Cat# J61904, Sigma, St. Louis, MO, USA) or L-Cystine (Cat# J61651, Sigma, St. Louis, MO, USA). Media was also supplemented with 10% FBS (Cat# 26140-079, Gibco, Grand Island, NY, USA), Hydrocortisone (Cat# H0135, Sigma, St. Louis, MO, USA), and Insulin-Transferrin-Selenium (Cat# 41400-045, Gibco, Grand Island, NY, USA).

Protocol for development of drug resistant cell line

H-MESO-1 cells were plated at 50% confluency and treated with TS starting at a concentration of 0.5 μM followed by repetitive drug treatment with a 48 h recovery period. The concentration of TS was gradually increased by 1.5-fold during tolerance selection until cells were no longer viable. Development of a drug-tolerant cell line at the EC_{50} (1 μM) was achieved within 2–3 months while achieving tolerance at 5 μM required 8 months of continued incremental treatment and limited dilution subcloning.

Knockdown of SLC7A11

H-MESO-1 cells were reverse transfected with Ambion Silencer Select Pre-Designed siRNA against SLC7A11(Cat# 4390824, lot A502KFIP Ambion/Invitrogen, Carlsbad, CA, USA) or a scramble siRNA (Cat#

4390843, lot A502K6LF and Cat# 4390846, lot A502HMU1 Ambion/Invitrogen, Carlsbad, CA, USA). Cells were diluted (300,000 cells/well for 6-well plates, 2,500 cells/well for 96-well plates) in antibiotic free complete growth medium in combination with RNAi duplex–Lipofectamine RNAiMax (Cat# 13778030, Thermo Fisher Scientific, Waltham, MA, USA) complex (1:1 ratio) in Opti-MEM (Cat# 51985091, Thermo Fisher Scientific, Waltham, MA, USA) according to the manufacturer's instructions (Thermo Fisher Scientific, Waltham, MA, USA) Transfected cells were plated in 6-well or 96-well plates (Corning Incorporated, Kennebunk, ME, USA) and incubated for 24–48 h before performing subsequent assays.

Cell viability assay and drug-drug synergy determination

Cell lines were plated at a density of 2500 cells/well in 96-well plates (Corning Incorporated, Kennebunk, ME, USA) and allowed to adhere overnight prior to treatment for 48 h with test compounds. Post-incubation cells were fixed with 3% formaldehyde (Fisher Bioreagents, Fair Lawn, NJ, USA) and stained with 0.1% crystal violet (Acros Organics, Fair Lawn, NJ, USA) as previously described[27]. Plates were imaged using a Lionheart plate reader (BioTek Instruments, Winooski, VT, USA) to determine total cell counts per well prior to the addition of methanol to solubilize the crystal violet. Absorbance was read at 540 nM. To determine the EC_{50} of test compounds the data were plotted using a 4-parameter non-linear regression model using GraphPad Prism7 or 10 software (GraphPad Software, San Diego, CA, USA). Resulting EC_{50} data were consistent across both cell enumeration and absorbance readings.

Live/dead assay

H-MESO-1 cells were plated in 6 well plates (Cat# 3516, Corning Incorporated, Kennebunk, ME, USA) and allowed to adhere overnight. Cells were treated with 1 μM thiostrepton for 18 h. The following day the Invitrogen Live/Dead reagents (Cat# R37601, Invitrogen, Carlsbad, CA, USA) were added to cells as per the manufacturer's instructions. Images were captured on an Eclipse TE-2000E inverted microscope (Nikon, Tokyo, Japan) equipped with a 20× objective and excited using the FITC and TRITC filter sets.

Western blotting

Cell lines were plated at a density of 150,000 cell/well in 6-well plates (Cat# 3516, Corning Incorporated, Kennebunk, ME, USA) and allowed to adhere overnight prior to treatment for 24 h with test compounds or incubation for 24 h for untreated controls. Cells were collected and lysed using RIPA lysis buffer (50 mM Tris-HCL, 150 mM NaCl, 1 mM EDTA, 1% Igepal CA-630, 0.25% sodium deoxycholate, 0.1% sodium dodecyl sulfate) and quantified using Pierce detergent compatible Bradford reagent (Cat# 1863028, Thermo Scientific, Rockford, IL, USA). Lysates (15ug/well) were resolved on Bis-Tris 4–12% gradient gels (Cat# WG140BX10, Invitrogen, Carlsbad, CA, USA) for 55 min at 200 V. Resolved proteins were transferred to an Amersham Hybond PVDF membrane (Cat# 10600023, Cytiva, Marlborough, MA, USA) for 90 min at 0.5 A followed by blocking in 5% bovine serum albumin (BSA) in Tris-buffered saline containing 1% Tween-20 (TBS-T) at room temperature for 2 h. Primary antibodies PRX3 1:2000 (Cat# LF-PA0225, AbFrontier, Seoul, Republic of Korea), SLC7A11 1:1000 (Cat# 12691S, Cell Signaling, Danvers, MA, USA), ACTB 1:3000 and GAPDH 1:3000 (Cat# MA5-11868 and Cat# MA5-15738, Invitrogen, Carlsbad, CA, USA), diluted in TBS-T were incubated overnight at 4 °C. After incubation, the membrane was washed in TBS-T for 1 h prior to the addition of the appropriate HRP-conjugated secondary antibody, anti-rabbit IgG HRP or anti-mouse IgG HRP 1:3000 (Cat# NA934 and Cat# NA931, GE HealthCare, Chicago, IL, USA). Western blots were then exposed to ECL Reagent (Cat#32209, Thermo Scientific, Rockford, IL, USA) and proteins visualized using a GE Amersham Imager (GE Healthcare, Chicago, IL, USA) and quantified by densitometry using ImageJ software (NIH, Bethesda, MD, USA). Antibody information found in Supplementary Table 4.

qRT-PCR

Cells were collected and RNA was isolated using the Qiagen RNeasy Plus Mini Kit (Cat# 74134, Qiagen, West Caldwell, NJ, USA) followed by generation of cDNA using Qiagen RT2 reverse transcription (Cat# 330404, Qiagen, West Caldwell, NJ, USA). qPCR was performed in a volume of 20 μl using the QuantStudio 3 Real Time Thermocycler and reactions took place in optical-grade, 96-well plates (Cat# 4483354, Applied Biosystems, Carlsbad, CA, USA) using Qiagen Universal SYBR Green Master (Cat# 330523, Qiagen, West Caldwell, NJ, USA). Relative mRNA levels were calculated as 2ΔCt. Equal cDNA loading was confirmed using two or more endogenous control primers (HPRT, PSMB4, GAPDH). Data are presented as the average of 2 or more biological replicates ± standard deviation. Validated primers were purchased from IDT (Integrated DNA Technologies, Coralville, IA, USA): SLC7A11 Cat# Hs.PT.58.4044772, HPRT Cat# Hs.PT.58 v.45621572, GAPDH Cat# Hs.PT.39a.22214836, PSMB4 (custom Fwd and Rev). Primer information found in Supplementary Table 5.

Compound treatment and ROS detection

The ROS-Glo H_2O_2 assay (Cat# G8820, Promega, Walldorf, Germany) was used to measure the level of H_2O_2 in culture after treatment with TS (2.5 μM) or erastin (2.5 μM) for 24 h following the manufacturer's instructions. Cells were plated at 2,500 cells/well in a 96-well plate (Cat# 3596 Corning Incorporated, Kennebunk, ME, USA) and incubated with or without glucose and H_2O_2 substrate solution for 4 h, followed by the addition of the RSO-Glo detection solution. Luminescence units were measured using measured using a BioTek plate reader (BioTek Instruments, Winooski, VT, USA).

Proliferation assay

Cell lines were plated at 25,000 cells/well in 6-well plates (Cat# 3516, Corning Incorporated, Kennebunk, ME, USA). Cells were trypsinized and collected every 24 h for 4 days and counted using a hemocytometer. Cell counts were graphed as cells/mL versus time.

Hyper7 transfection and image analysis

Cell lines were plated at a density of 200,000 cells/well in a 6-well plate (Cat# 3516, Corning Incorporated, Kennebunk, ME, USA) on top of a glass coverslip and allowed to adhere overnight. Post 24 h, cells were transfected at a 2:1 ratio of X-tremeGENE (Cat# XTG9-RO, Roche, Basel, Switzerland) to plasmid (pCS2+MLS-HyPer7, Addgene #136470 or pCS2+IMS-HyPer7, Addgene #136469) and incubated at 37 °C for 48 h. After 48 h images were captured on an Eclipse TE-2000E inverted microscope (Nikon, Tokyo, Japan) equipped with a 40×/1.3 numerical aperture (NA) Plan Fluor oil-immersion objective and excited at 470 nm and 440 nm. HyPer7 oxidation was calculated by dividing the fluorescence intensity at 470 nm by the intensity at 440 nm.

Colony formation assay

Cell lines were plated at a density of 1000 cell/well in 6-well plates (Cat# 3516, Corning Incorporated, Kennebunk, ME, USA) and incubated for 11 days at 37 °C. After 11 days wells were washed with 1X PBS and stained with 0.1% crystal violet (Cat# 229641000, Acros Organics, Fair Lawn, NJ, USA) for 15 mins.

Seahorse assay

The mitochondrial oxygen consumption rates (OCR) and extracellular acidification rates (ECAR) were evaluated for each PRX3 KO cell line and Ctrl using the Extracellular Flux Analyzer XF24 (Seahorse Biosciences, North Billerica, MA, USA). Cells were plated in 96-well plates (Cat# 3596, Corning Incorporated, Kennebunk, ME, USA) at a density of 9000 cells/well and allowed to adhere for 24 h. Measurements were

performed according to the manufacturer's directions with the replacement of growth media with serum-free XF assay medium (Cat# 103575-100, Seahorse Biosciences, North Billerica, MA, USA), and the placement of a cartridge equipped with oxygen-sensitive and pH-sensitive probes (Seahorse Biosciences, North Billerica, MA, USA) above the cells. OCR, indicative of mitochondrial respiration and ECAR, indicative of glycolysis were evaluated after injection of oligomycin at 1 μM, carbonyl cyanide-*p*-trifluoromethoxyphenylhydrazone (FCCP) at 1 μM, and rotenone and antimycin A at 0.5 μM. OCR and ECAR values were calculated using the Seahorse Wave software. The XF software computes OCR from the fall in O_2 tension during each 2–5 min measurement period and reports the rate directly.

Xenograft model of human Mesothelioma

Male Fox Chase (CB17/lcr-Prkdcscid/lcrlcoCr background) severe combined immunodeficient (SCID) mice, aged between 6 and 8 weeks old (Charles River Laboratories, Wilmington, MA) were injected intraperitoneal (IP) with 2×10^6 H-MESO-1 Ctrl or PRX3 KO clone cells into the lower left quadrant and tumors were allowed to form for 41 days. Mouse weight was monitored once a week and after 5 weeks, mice were euthanized. Mice did not lose >10% of body weight which would require euthanasia via protocol. Free-floating spheroidal and mesenteric tumors were recovered by surgical resection, and tumor weight was measured in grams (g). Tumor tissue was fixed in 4% paraformaldehyde in phosphate buffered solution (PBS) for processing and immunohistochemical assays.

Patient-derived explants (PDEs) model of mesothelioma

Tumor samples were collected for research following informed patient consent and ethical approval (Research Ethics Committee - 14/LO/1527). Upon collection, samples were placed into pre-cooled Hank's Balanced Salt Solution (HBSS) and processed into cubical-shaped explants (~1–8mm^3) within 3 h. An aliquot of each tumor sample was immediately snap-frozen to provide baseline (untreated, uncultured) tissue for RNA extraction and sequencing. Explants were cultured at 37 °C with 10% CO_2 in RPMI media with 1X GlutaMAX (100x solution, Cat# 35050061, Gibco, Grand Island, NY, USA), 10% FBS (Cat# 26140-079, Gibco, Grand Island, NY, USA), 1% penicillin-streptomycin (10,000 U/mL penicillin, 10,000 μg/mL streptomycin; Cat# 15140122, Gibco, Grand Island, NY, USA), and 1% amphotericin B (250 μg/mL, Cat# 15290026, Gibco, Grand Island, NY, USA). Explants were allowed to adapt for 16–24 h before treatment. Fresh media containing 5 μM, 10 μM and 100 μM of TS as well as without additive was used to replace previous media after adaptation period. Duplicate sets were prepared for each treatment condition. One set was harvested and snap-frozen for future RNA extraction after 24 h of treatments. The other set was processed into formalin fixed paraffin embedded (FFPE) blocks after 48 h.

RNA extraction and sequencing

RNA extraction was performed on samples from the baseline (untreated, uncultured) tumor tissue collected at the time of explant preparation, as well as from untreated control and the 10 μM TS-treated explants. Tissues were homogenized using Gentle MACS Dissociator (Miltenyi Biotech, Bergisch Gladbach, Germany) followed by RNA isolation using the Monarch Total RNA Miniprep Kit (Cat# T2010S, New England Biolabs, Ipswich, MA, USA) as indicated in manufacturer's protocol. RNA concentrations were determined using Qubit High Sensitivity (HS) RNA Assay Kit and Qubit 4.0 Fluorometer. The extracted RNA samples were then submitted for sequencing. RNA-seq libraries were prepared using polyA selection and sequenced on an Illumina platform employing paired-end (PE) 150 bp reads. Each sample generated approximately 20 million PE reads, corresponding to roughly 6 Gb of sequencing data per sample. The sequencing output was processed, and results were provided as read count matrices for downstream analysis.

Multiplex immunofluorescence (mIF) and image analysis

Sections from FFPE processed explants were stained using Opal 4-Color Manual IHC Kit (Cat# NEL810001KT, Akoya Biosciences, Boston, MA, USA) according to manufacturer's instructions. The following antibodies were used: i) cleaved poly(ADP-ribose) polymerase-1 (cPARP) (Cat# ab32064, clone E51, Abcam, Cambridge, UK) to assess cell death; ii) Ki67 (Cat# M724029, clone MIB1, Agilent, Santa Clara, CA, USA) to evaluate proliferation and iii) pan-cytokeratin (Cat# M082102, clone MNF116, Agilent, Santa Clara, CA, USA) as a guide for a training tumor stroma classifier. Selected tissue sections were stained with an additional panel consisting of SLC7A11 (Cat# ab307601, clone EPR27115-64, Abcam, Cambridge, UK) and pan-cytokeratin (Cat# M082102, clone MNF116, Agilent, Santa Clara, CA, USA) to qualitatively assess differences in protein levels between TS-treated and control explants. Image analysis for assessment of differences in cPARP levels between treatment conditions was carried out using Inform software for spectral unmixing, followed by QuPath[55] for cell detection and phenotyping. Tumor and stromal regions were segmented using an Artificial Neural Network (ANN)-based classifier, which leveraged morphological features, DAPI staining, and autofluorescence signals to differentiate tissue compartments. Threshold was applied to quantify nuclear positivity for cPARP. The percentage of positive tumor cells was calculated for each explant containing over 100 tumor cells. Quantitative analysis of cPARP-positive tumor cells was used as the input for assessment of treatment-induced cell death.

Assessment of treatment-induced cell death

To enable quantitative assessment of treatment-induced cell death across heterogeneous explant cultures, a weighted response score (WRS) was calculated for each case. The WRS integrates cPARP induction data across all TS doses (5, 10, 100 μM) for each tumor donor. This approach accounts for differences in the number of available and analyzable explants per group (defined as samples with ≥ 100 tumor cells), reflecting tissue variability between cases and conditions. The metric is based on Kruskal–Wallis test and was designed to capture cPARP induction relative to control across multiple TS concentrations, thereby enabling detection of differences that may not be observed when evaluating a single concentration. WRS provides a consistent and interpretable summary for comparison across cases. Accordingly, WRS is intended as a ranked summary of multi-dose cPARP induction across explants. Briefly, the Kruskal–Wallis test was applied to the cPARP staining results to obtain Kruskal–Wallis statistic (H) and *p*-value. To estimate the proportion of variance explained by the treatment, the effect size (ε^2) was calculated using following formula: $\varepsilon^2 = (H - (k - 1))/(n\text{-}k)$. Where: H=Kruskal–Wallis statistic, k= number of treatment groups, n= total number of observations (explants). As a next step the difference of medians for each treatment condition was obtained by subtracting the median of the control group from the median of the matching treated group, followed by calculation of weights: weight= number of explants in one treatment group/n. This weighting accounts for differences in the number of analyzable explants per condition, ensuring that conditions represented by fewer observations do not disproportionately influence the overall score. The weighted difference for each treatment was then computed by multiplying the median difference by its corresponding weight and sum of these weights was treated as total weighted difference across treatment conditions. Next, weighted response score for each case was calculated using following formula: $WRS = \varepsilon^{2*}(-\log_{10}(p - value))$*total weighted difference. To normalize the WRS values, a robust Z-score was calculated using the median and Median Absolute Deviation (MAD) as follows: Robust Z-score = (WRS−median)/(MAD*1.4826). This single interpretable value allowed for assignment samples into two groups: R with Robust Z-score <0 and NR with Robust Z−score ≥ 0.

RNAseq data analysis

RNA-seq libraries were prepared using polyA selection and sequenced on an Illumina platform with 150 bp paired-end (PE) reads. Approximately 20 million PE reads were generated per sample, resulting in about 6 Gb of data for each sample. The data were provided as read count matrices for further analysis. Differential expression analysis was performed using the DESeq2 package (version 1.42.1) in R[56]. The median-of-ratios method was applied for normalization, and statistical significance was determined using Wald tests. P-values were adjusted for multiple testing using the Benjamini–Hochberg method to control the false discovery rate. Genes with an adjusted p-value (padj) <0.05 were considered significantly differentially expressed. Gene set enrichment analysis (GSEA) was carried out using the fast gene set enrichment analysis (FGSEA) package (version 1.28.0) in R[57]. Genes were ranked based on the Wald statistic from the DESeq2 results, and the FGSEA function was executed with 1,000 permutations to identify enriched gene sets.

Whole exome sequencing and data analysis

Whole exome sequencing (WES) and data analysis were performed as described previously[58]. Genomic DNA was extracted from diagnostic FFPE tumor blocks and buffy coat samples collected from the same patients who donated tissue for explant studies. Library preparation for WES was completed using the Agilent SureSelect Human All Exon V6 kit (Cat# 5190-8865, Agilent, Santa Clara, CA, USA), and sequencing was performed on the Illumina NovaSeq 6000 platform, generating 150 bp PE reads. Sequencing reads were processed with FASTP for quality control before alignment to the hg19 human reference genome using Burrows-Wheeler Aligner (BWA). Picard tools were applied to mark duplicate reads, and somatic variants, including single nucleotide variants (SNVs) and insertions/deletions (INDELs), were identified using both MuTect2 and VarScan2. Variant annotation was conducted with ANNOVAR to assess functional impact. Variants were considered for analysis if detected by both variant callers with a variant allele frequency (VAF) greater than 2%, or solely by VarScan2 with VAF exceeding 5%. Variants located within repetitive regions or those with a population frequency above 1% in 1000 Genomes, the Exome Aggregation Consortium (EXAC), or the NHLBI Exome Sequencing Project (ESP6500) databases were excluded. Somatic copy number alterations (SCNAs) were detected using allele-specific copy number analysis of tumors (ASCAT), with additional refinement of tumor purity and ploidy assessments through manual curation of outputs from ABSOLUTE. The finalized data were compiled into patient- specific datasets, detailing SCNAs by genomic loci and SNVs by gene.

Statistical analysis

Statistical analyses were conducted using Graph Pad Prism (unless stated otherwise) and adapted to the type and distribution characteristics of each dataset. Normality for quantitative variables was assessed by the Shapiro–Wilk test. Where any sample within a comparison deviated from normality, nonparametric tests were applied. Independent samples were compared using the two-sided Mann–Whitney or Kruskal–Wallis test, depending on the number of groups. Paired samples were analyzed with the Wilcoxon signed – rank test. Fisher's exact test was used for categorical data in contingency tables. Survival analyses were performed using Kaplan–Meier with log-rank tests. For association between continuous variables nonparametric Spearman's rank test was applied with Spearman r and two-tailed p value reported. All above analyses were hypothesis-driven, targeting a maximum of two group comparisons per test. As such, no multiple testing correction was performed. For DESeq2 differential expression and fgsea gene set enrichment, multiple comparison correction was applied using the Benjamini–Hochberg method. Significance for all tests was set at $p < 0.05$, or at adjusted $p < 0.05$ for FDR-corrected analyses. The applied tests are indicated in text.

Phase 1 clinical testing of RSO-021 (MITOPE)

Related trial information can be found at clinicaltrials.gov where the trial is registered as NCT05278975. The complete trial protocol can be found in the supplemental information. The phase 1 portion of the trial has ended. Preliminary data were presented at the 2024 American Society for Clinical Oncology Conference with the related abstract (Fennell et al. J Clin Oncol 42, 3019-3019(2024)). The trial design and conduct of the trial complied with all relevant regulations regarding the use of human study participants and were conducted in accordance with the criteria set by the Declaration of Helsinki. The trial was reviewed and approved by the Medicines and Healthcare products Regulatory Agency (MHRA).

Reporting summary

Further information on research design is available in the Nature Portfolio Reporting Summary linked to this article.

Data availability

The data that support the findings of this study are available in the source file. The Whole Exome Sequencing (WES) FFPE dataset have been deposited in the European Genome-phenome Archive (EGA) (https://ega-archive.org/) and assigned the study accession: EGAS50000001813 and dataset accession: EGAD50000002620. The RNA-Seq data has been deposited in the EGA and assigned the study accession number: EGAS50000001827 and dataset accession: EGAD50000002650. All other data supporting this work are available in main article, supplementary information or source data file. Source data is provided with this manuscript. Source data are provided with this paper.

References

1. Luo, J., Solimini, N. L. & Elledge, S. J. Principles of cancer therapy: oncogene and non-oncogene addiction. *Cell* **136**, 823–837 (2009).
2. Weinberg, F. & Chandel, N. S. Mitochondrial metabolism and cancer. *Ann. N. Y Acad. Sci.* **1177**, 66–73 (2009).
3. Weinberg, F. & Chandel, N. S. Reactive oxygen species-dependent signaling regulates cancer. *Cell Mol. Life Sci.* **66**, 3663–3673 (2009).
4. Schieber, M. & Chandel, N. S. ROS function in redox signaling and oxidative stress. *Curr. Biol.* **24**, R453–R462 (2014).
5. Janes, S. M., Alrifai, D. & Fennell, D. A. Perspectives on the treatment of malignant pleural mesothelioma. *N. Engl. J. Med* **385**, 1207–1218 (2021).
6. Yang, H. et al. MEK1 drives oncogenic signaling and interacts with PARP1 for genomic and metabolic homeostasis in malignant pleural mesothelioma. *Cell Death Discov.* **9**, 55 (2023).
7. Urso, L. et al. Metabolic rewiring and redox alterations in malignant pleural mesothelioma. *Br. J. Cancer* **122**, 52–61 (2020).
8. Gorrini, C., Harris, I. S. & Mak, T. W. Modulation of oxidative stress as an anticancer strategy. *Nat. Rev. Drug Discov.* **12**, 931–947 (2013).
9. Cunniff, B. et al. Disabling mitochondrial peroxide metabolism via combinatorial targeting of peroxiredoxin 3 as an effective therapeutic approach for malignant mesothelioma. *PLoS One* **10**, e0127310 (2015).
10. Cunniff, B. et al. Peroxiredoxin 3 levels regulate a mitochondrial redox setpoint in malignant mesothelioma cells. *Redox Biol.* **3**, 79–87 (2014).
11. Cunniff, B. et al. Mitochondrial-targeted nitroxides disrupt mitochondrial architecture and inhibit expression of peroxiredoxin 3 and FOXM1 in malignant mesothelioma cells. *J. Cell Physiol.* **228**, 835–845 (2013).
12. Kinnula, K. et al. Endogenous antioxidant enzymes and glutathione S-transferase in protection of mesothelioma cells against hydrogen peroxide and epirubicin toxicity. *Br. J. Cancer* **77**, 1097–1102 (1998).

13. Newick, K. et al. Peroxiredoxin 3 is a redox-dependent target of thiostrepton in malignant mesothelioma cells. *PLoS One* **7**, e39404 (2012).
14. Hall, A., Karplus, P. A. & Poole, L. B. Typical 2-Cys peroxiredoxins-structures, mechanisms and functions. *FEBS J.* **276**, 2469–2477 (2009).
15. Stein, K. T. et al. Kinetic modeling of H2O2 dynamics in the mitochondria of HeLa cells. *PLoS Comput Biol.* **16**, e1008202 (2020).
16. Wood, Z. A. et al. Structure, mechanism and regulation of peroxiredoxins. *Trends Biochem Sci.* **28**, 32–40 (2003).
17. Kinnula, V. L. et al. Overexpression of peroxiredoxins I, II, III, V, and VI in malignant mesothelioma. *J. Pathol.* **196**, 316–323 (2002).
18. Nelson, K. J., et al., Unique cellular and biochemical features of human mitochondrial peroxiredoxin 3 establish the molecular basis for its specific reaction with thiostrepton. *Antioxidants (Basel)* **10**, 150 (2021).
19. Pak, V. V. et al. Ultrasensitive genetically encoded indicator for hydrogen peroxide identifies roles for the oxidant in cell migration and mitochondrial function. *Cell Metab.* **31**, 642–653 e6 (2020).
20. Qiao, S. et al. Thiostrepton is an inducer of oxidative and proteotoxic stress that impairs viability of human melanoma cells but not primary melanocytes. *Biochem Pharm.* **83**, 1229–1240 (2012).
21. Tsherniak, A. et al. Defining a cancer dependency map. *Cell* **170**, 564–576 e16 (2017).
22. Zhang, M. et al. Clonal architecture in mesothelioma is prognostic and shapes the tumour microenvironment. *Nat. Commun.* **12**, 1751 (2021).
23. Ianevski, A., Giri, A. K. & Aittokallio, T. SynergyFinder 2.0: visual analytics of multi-drug combination synergies. *Nucleic Acids Res.* **48**, W488–W493 (2020).
24. Dixon, S. J. et al. Pharmacological inhibition of cystine-glutamate exchange induces endoplasmic reticulum stress and ferroptosis. *Elife* **3**, e02523 (2014).
25. Stockwell, B. R. et al. Ferroptosis: a regulated cell death nexus linking metabolism, redox biology, and disease. *Cell* **171**, 273–285 (2017).
26. Cunniff, B. et al. A direct and continuous assay for the determination of thioredoxin reductase activity in cell lysates. *Anal. Biochem* **443**, 34–40 (2013).
27. Nonn, L., Berggren, M. & Powis, G. Increased expression of mitochondrial peroxiredoxin-3 (thioredoxin peroxidase-2) protects cancer cells against hypoxia and drug-induced hydrogen peroxide-dependent apoptosis. *Mol. Cancer Res* **1**, 682–689 (2003).
28. Wang, X. Y., Wang, H. J. & Li, X. Q. Peroxiredoxin III protein expression is associated with platinum resistance in epithelial ovarian cancer. *Tumour Biol.* **34**, 2275–2281 (2013).
29. Arafeh, R. et al. The present and future of the cancer dependency map. *Nat. Rev. Cancer* **25**, 59–73 (2025).
30. Huh, J. Y. et al. Peroxiredoxin 3 is a key molecule regulating adipocyte oxidative stress, mitochondrial biogenesis, and adipokine expression. *Antioxid. Redox Signal* **16**, 229–243 (2012).
31. Li, L. et al. Increased susceptibility of MER5 (peroxiredoxin III) knockout mice to LPS-induced oxidative stress. *Biochem Biophys. Res. Commun.* **355**, 715–721 (2007).
32. Whitaker, H. C. et al. Peroxiredoxin-3 is overexpressed in prostate cancer and promotes cancer cell survival by protecting cells from oxidative stress. *Br. J. Cancer* **109**, 983–993 (2013).
33. Song, I. S. et al. Mitochondrial peroxiredoxin III is a potential target for cancer therapy. *Int J. Mol. Sci.* **12**, 7163–7185 (2011).
34. Blyth, K. G. et al. Leveraging the pleural space for anticancer therapies in pleural mesothelioma. *Lancet Respir. Med* **12**, 476–483 (2024).
35. Bhatnagar, R. & Maskell, N. A. Indwelling pleural catheters. *Respiration* **88**, 74–85 (2014).
36. Zhou, Q. et al. Ferroptosis in cancer: from molecular mechanisms to therapeutic strategies. *Signal Transduct. Target Ther.* **9**, 55 (2024).
37. Koppula, P., Zhuang, L. & Gan, B. Cystine transporter SLC7A11/xCT in cancer: ferroptosis, nutrient dependency, and cancer therapy. *Protein Cell* **12**, 599–620 (2021).
38. Badgley, M. A. et al. Cysteine depletion induces pancreatic tumor ferroptosis in mice. *Science* **368**, 85–89 (2020).
39. Liu, T. et al. The deubiquitylase OTUB1 mediates ferroptosis via stabilization of SLC7A11. *Cancer Res* **79**, 1913–1924 (2019).
40. Yan, Y. et al. SLC7A11 expression level dictates differential responses to oxidative stress in cancer cells. *Nat. Commun.* **14**, 3673 (2023).
41. Rahim, S. & Uren, A. A real-time electrical impedance based technique to measure invasion of endothelial cell monolayer by cancer cells. *J. Vis. Exp.* **50**, 2792 (2011).
42. Testa, J. R. et al. Germline BAP1 mutations predispose to malignant mesothelioma. *Nat. Genet* **43**, 1022–1025 (2011).
43. Bueno, R. et al. Comprehensive genomic analysis of malignant pleural mesothelioma identifies recurrent mutations, gene fusions and splicing alterations. *Nat. Genet* **48**, 407–416 (2016).
44. Hiltbrunner, S. et al. Genomic landscape of pleural and peritoneal mesothelioma tumours. *Br. J. Cancer* **127**, 1997–2005 (2022).
45. Hmeljak, J. et al. Integrative molecular characterization of malignant pleural mesothelioma. *Cancer Discov.* **8**, 1548–1565 (2018).
46. Zhang, Y., Koppula, P. & Gan, B. Regulation of H2A ubiquitination and SLC7A11 expression by BAP1 and PRC1. *Cell Cycle* **18**, 773–783 (2019).
47. Xu, D. et al. BAP1 deficiency inflames the tumor immune microenvironment and is a candidate biomarker for immunotherapy response in malignant pleural mesothelioma. *JTO Clin. Res Rep.* **5**, 100672 (2024).
48. Fahey, C. C. & Davis, I. J. SETting the stage for cancer development: SETD2 and the consequences of lost methylation. *Cold Spring Harb. Perspect Med.* **7**, a026468 (2017).
49. Guo, S. et al. Interplay between H3K36me3, methyltransferase SETD2, and mismatch recognition protein MutSalpha facilitates processing of oxidative DNA damage in human cells. *J. Biol. Chem.* **298**, 102102 (2022).
50. Carvalho, S. et al. SETD2 is required for DNA double-strand break repair and activation of the 53-mediated checkpoint. *Elife* **3**, e02482 (2014).
51. Hu, K. et al. Suppression of the SLC7A11/glutathione axis causes synthetic lethality in KRAS-mutant lung adenocarcinoma. *J. Clin. Invest* **130**, 1752–1766 (2020).
52. Papa, S. et al. Phase 2 study of sorafenib in malignant mesothelioma previously treated with platinum-containing chemotherapy. *J. Thorac. Oncol.* **8**, 783–787 (2013).
53. Zheng, J. et al. Sorafenib fails to trigger ferroptosis across a wide range of cancer cell lines. *Cell Death Dis.* **12**, 698 (2021).
54. Nelson, K. J. et al. Mechanism-based peroxiredoxin 3 inhibitors exploit a covalent warhead for cancer therapy. *Sci. Adv.* **11**, eady4492 (2025).
55. Bankhead, P. et al. QuPath: open source software for digital pathology image analysis. *Sci. Rep.* **7**, 16878 (2017).
56. Love, M. I., Huber, W. & Anders, S. Moderated estimation of fold change and dispersion for RNA-seq data with DESeq2. *Genome Biol.* **15**, 550 (2014).
57. Korotkevich, G. et al. Fast gene set enrichment analysis. *bioRxiv*, 060012. https://doi.org/10.1101/060012 (2021)
58. Zhang, M. et al. A gut microbiota rheostat forecasts responsiveness to PD-L1 and VEGF blockade in mesothelioma. *Nat. Commun.* **15**, 7187 (2024).

Acknowledgements
We thank the patients for their participation in this research and their families for their support. Part of this study was carried out at the National Institute for Health and Care Research (NIHR) Leicester BRC (NIHR203327). We thank the Advanced Imaging Facility (RRID:SCR_020967) at the University of Leicester for their support. We thank Dr. Alan Howe (UVM) for generous use of his microscope. We thank the UVM Cancer Center for their support. We thank the Butler Family Foundation for their support.

Author contributions
V.G., J.D., T.M., A.B., C.P., J.R., J.C.H., A.H., S.S., A.S., M.Z., A.N., P.W., K.K., K.J.B., N.H.H., G.N.N., M.D., D.A.F. and B.C. collected samples, conducted experiments, and analyzed data. G.N.N., S.D., J.S., D.A.F. and B.C. conceived and designed the trial in collaboration with RS Oncology. K.G.B., P.W.S., S.L., F.T., J.H.C., B.A., S.D., J.S., D.A.F. collected clinical data. V.G., J.D., T.M., J.S., D.A.F., and B.C. wrote the paper, and all authors edited the paper.

Funding
This work was funded by RS Oncology, LLC through a Sponsored Research Contract to the University of Vermont and the University of Leicester. The MITOPE study is sponsored by RS Oncology, LLC. V.G. was supported in part by the University of Vermont Cancer Center, the Vermont Lung Center, and the Butler Family Foundation. The authors acknowledge additional financial support from the UK Department of Health and Cancer Research UK via Experimental Cancer Medicine Center awards to King's Health Partners/Guy's & St Thomas' NHS Foundation Trust (JS).

Competing interests
T.M., B.C., G.N.N., and D.A.F. are paid consultants and B.C. and N.H.H. are equity holders in RS Oncology, LLC. K.G.B. has received consultancy fees and institutional funding for research from RS Oncology. B.C. is an inventor on a patent (WO2020142782A1) submitted by RS Oncology, University of Vermont, and Wake Forest University Health Sciences that covers use of an intact thiostrepton formulation for the treatment of cancer. The remaining authors declare no competing interests.

Additional information
Supplementary information The online version contains supplementary material available at https://doi.org/10.1038/s41467-026-75153-y.

Correspondence and requests for materials should be addressed to James Spicer, Dean A. Fennell or Brian Cunniff.

Peer review information *Nature Communications* thanks Liron Bar-Peled and the other anonymous reviewer(s) for their contribution to the peer review of this work. A peer review file is available.

Reprints and permissions information is available at http://www.nature.com/reprints

Publisher's note Springer Nature remains neutral with regard to jurisdictional claims in published maps and institutional affiliations.

[1]Department of Pathology and Laboratory Medicine, University of Vermont Cancer Center, Larner College of Medicine, Burlington, VT, USA. [2]UK National Institute for Health Research Biomedical Research Centre & Cancer Research UK Experimental Cancer Medicine Centre, Mesothelioma Research Programme, University of Leicester, Leicester, UK. [3]Centre for Cell Death, Cancer, and Inflammation (CCCI), UCL Cancer Institute, University College London, London, UK. [4]School of Cancer Sciences, University of Glasgow, Glasgow, UK. [5]Barts and the London NHS Trust, London, UK. [6]Department of Oncology, University of Oxford, Oxford, UK. [7]The Christie NHS Foundation Trust, Manchester, UK. [8]Novogene, Beijing, China. [9]University Hospitals of Leicester, Leicester, UK. [10]RS Oncology, LLC, Cambridge, MA, USA. [11]King's College London, Guy's Hospital, London, UK. [12]Division of Cancer Sciences, University of Leicester, Leicester, UK. [13]These authors contributed equally: Victoria Gibson, Joanna Dzialo, Terri Messier. [14]These authors jointly supervised this work: James Spicer, Dean A. Fennell, Brian Cunniff. ✉e-mail: james.spicer@kcl.ac.uk; df132@leicester.ac.uk; bcunniff@uvm.edu